Biodegradable Nanocomposite Developed from the PLA/PCL Blends and Silk Fibroin Nanoparticle: Study on the Microstructure, Thermal Behavior, Crystallinity, and Performance

Masoud Dadras Chomachayi[1], Azam Jalali-arani[2*], Freddys R. Beltrán[3, 4], Mª Ulagares de la Orden[4, 5], Joaquín Martínez Urreaga[3, 4]

[1]Mahshahr Campus, Amirkabir University of Technology, P.O. Box 63517-13178, Mahshahr, Iran

[2] Department of Polymer Engineering & Color Technology, Amirkabir University of Technology, P.O. Box 15875-4413, Tehran, Iran

[3] Departamento de Ingeniería Química Industrial y del Medio Ambiente, E.T.S.I. Industriales, Universidad Politécnica de Madrid, José Gutiérrez Abascal 2, 28006 Madrid, Spain

[4] Grupo de Investigación ''Polímeros: Caracterización y Aplicaciones (POLCA)'' (Unidad Asociada ICTP-CSIC), E.T.S.I. Industriales, Universidad Politécnica de Madrid, José Gutiérrez Abascal 2, 28006 Madrid, Spain

[5] Departamento de Química Orgánica, Universidad Complutense de Madrid, Facultad de Óptica y Optometría, Arcos de Jalón 118, 28037 Madrid, Spain

*Corresponding Author:

Azam Jalali-arani

Department of Polymer Engineering & Color Technology,

Amirkabir University of Technology (Tehran Polytechnic)

E-mail: ajalali@aut.ac.ir

Tel: + 98 21 64542435

Abstract

Recently, the use of natural materials has grown in the plastics industry. In this study, silk fibroin nanoparticle (SFNP) was successfully synthesized from silk fibroin (SF) and analyzed by Fourier-transform infrared spectroscopy (FT-IR), X-ray diffraction (XRD), thermogravimetric analysis (TGA), and differential scanning calorimetry (DSC). The obtained results revealed that the well-ordered domains in SF were changed to an amorphous structure in SFNP and it was attributed to the cleavage of SF polypeptide chains upon acid hydrolysis. Then several blends of poly(lactic acid)/poly(Ɛ-caprolactone) (PLA/PCL) containing different amounts of PCL were prepared and characterized. Based on the test results the best properties were achieved in the blend with 30% of PCL. The addition of 1% of SFNP into this blend enhanced the compatibility between PLA and PCL and reduced the PCL droplet size from 1.170±92 μm to 794±46 nm, this was observed by scanning electron microscopy (SEM). Thermal analysis indicated that the presence of SFNP caused an improvement of thermal degradation stability of the PLA/PCL blend in the end set temperature range. The crystallization process also slowed and the crystal growth rate decreased from 0.34 to 0.31 min^{-1}. Additionally, the use of SFNP increased (9.7%) the hardness value and reduced (15.7%) the water vapor permeability value of the PLA/PCL blend. The results of these experiments demonstrated that the prepared PLA/PCL/SFNP green nanocomposites have good potential for the food packaging applications.

Key words:

Poly(lactic acid); Poly(Ɛ-caprolactone); Silk fibroin nanoparticle; Microstructure; Thermal behavior; Barrier properties

1. Introduction

Over the last few decades, the wide use of oil-based and non-degradable plastic products has led to serious environmental pollution [1]. Specifically, the packaging industry produces a huge amount of waste plastic in some critical areas [2]. One of the proposed solutions to those problems is the use of bio-based polymers, which are produced from renewable resources and have been attracting much attention in recent years [3]. One of the most popular examples of bio-based plastic which are widely used in the market is poly(lactic acid) (PLA). PLA is produced from ring-opening polymerization of lactide monomer [4], and has many potential advantages, such as good processability, stiffness, thermal plasticity, and excellent physical and optical properties [5]. The low elongation at break (~ 3%) is one of the major drawbacks of PLA, which limits its utilization in demanding applications [6].

The aforementioned drawback has brought to the fore the need of sustainable methods for toughening of PLA without losing its other good properties. In this regard, many investigations have been carried out to increase the ductility of PLA via plasticization. However, plasticizers rapidly migrate to the surface, which could be a problem in some applications [7]. Polymer blending is the most widely accepted and economically viable method to obtain new materials with enhanced performance by combining properties of each polymer [8]. The blending of PLA with more flexible polymers, such as poly(Ɛ-caprolactone) (PCL), allows optimizing the performance of the plastic. PCL is a biodegradable polyester and has important advantages, such as good biodegradability, biocompatibility, and flexibility, allowing its use in the packaging and

medical applications [9][10][11][12]. However, these polymers are thermodynamically immiscible and phase separation would lead to the probable deterioration of the polymer blend properties [13].

Various methods have been studied to modify the morphology of the PLA/PCL blend and increase the compatibility between the polymer phases, such as the addition of multi-block copolymer, reactive polymers, multi-functional polymeric compatibilizers, and fillers [14]. Recently, it was proposed that the incorporation of nanoparticles into the polymer blends would effectively confer multifunctional enabling properties. Hoidy et al. studied the effect of an organoclay (OMMT) on the morphology and properties of the PLA/PCL blends. The SEM results showed that the addition of OMMT strongly affected the morphology and decreased the PCL domain size. Additionally, nanoparticles improved the thermal stability and tensile properties of the nanocomposites [15]. Decol et al. investigated the effect of the titanium dioxide (TiO$_2$) nanoparticles in the PLA/PCL blend. The results indicated that the nanoparticle acted as a compatibilizer due to its localization at the phase interface and improved interfacial adhesion between the two polymers [16]. Moreover, Bouakaz et al. used a hybrid of OMMT/graphene to increase the functional properties of the PLA/PCL blend. The obtained results showed that the miscibility of the blend was improved in the presence of the hybrid filler. Furthermore, this PLA/PCL nanocomposite exhibited higher thermal stability and barrier properties than the neat polymer blend [10].

Nowadays, fully degradable composites reinforced with organic nanoparticles and bio-fillers have a major attraction for the preparation of industrial products [17][18]. Organic nanoparticles extracted from renewable resources have been found as interesting fillers, showing different

4

specifications. Their availability, biocompatibility, biodegradability, and low cost makes them suitable for the fabrication of green polymer composites [19].

Silk fibroin nanoparticles are a promising kind of nanoparticles. They are produced from silk fibroin (SF), a highly abundant natural polymer that is extracted from the cocoon of the *bombyx mori* silkworm and has been used as reinforcements for engineering plastics due to their unique mechanical properties, non-toxicity, biodegradability, lightweight, and low cost [20][21]. To the best of our knowledge, there is little information on the effects of SFNP on the morphology and properties of the PLA/PCL blends in the literature. Consequently, the main aim of this research is to study the PLA/PCL/SFNP bio-nanocomposites prepared by melt blending. The characterizations of samples were done by scanning electron microscopy (SEM), Fourier-transform infrared spectroscopy (FT-IR), and differential scanning calorimetry (DSC). Thermal stability, mechanical, and transport properties were studied by using thermogravimetric analysis (TGA), Vicker microhardness, and water vapor permeability (WVP), respectively.

2. Materials and methods

2.1. Materials

Bombyx mori silkworm cocoons were obtained from the University of Guilan (Rasht, Iran). Sodium carbonate (Na_2CO_3) and chloroform were purchased from Merck (Germany). Sulfuric acid (95-97 %) was purchased from Honeywell (USA). Cellulose tube dialysis membrane (SnakeSkin® Dialysis Tubing, 3,500 Molecular Weight Cutoff (MWCO)) was purchased from Thermo Fisher Scientific (USA). A commercial-grade of PLA (Ingeo 2003D, Natureworks®),

with a melt mass-flow rate of 6 g/10 min (2.16 kg at 210 °C) was used. PCL Capa^{TM} 6800, with a melt flow index of 3 g/10 min (2.16 kg at 160 °C) was kindly supplied by Perstorp (Sweden).

2.2. Preparation of silk fibroin nanoparticles (SFNP)

Firstly, *Bombyx mori* silkworm cocoons (5 g) were boiled twice in a 0.5% (W/V) Na_2CO_3 solution for 30 min at 98 °C and then rinsed several times in distilled water (until pH became constant) to completely remove the sericin and other impurities and obtain silk fibroin (SF). The degummed SF was dried overnight at 50 °C in a vacuum oven to remove water [20][23]. Silk fibroin nanoparticles (SFNP) were obtained by the acid hydrolysis of SF with a sulfuric acid aqueous solution (64 wt%) at 45 °C under continuous stirring [24]. The SF-to-acid ratio was 1:10 (1 g of SF in 10 ml of H_2SO_4). The hydrolysis was stopped after 2 h of reaction by adding 50 ml of distilled water [25]. Then, the mixture was cooled down to room temperature and centrifuged five times at 5,000 rpm for 15 min to remove the excess of acids. The hydrolysate SF was dialyzed in a dialysis membrane against distilled water for 4 days by changing the water several times for the removal of the non-reactive sulfate groups and salts. Finally, the dispersion of SFNP was freeze-dried to obtain dried SFNP powder. Figure 1 shows the schematic image of the method for the preparation of SFNP.
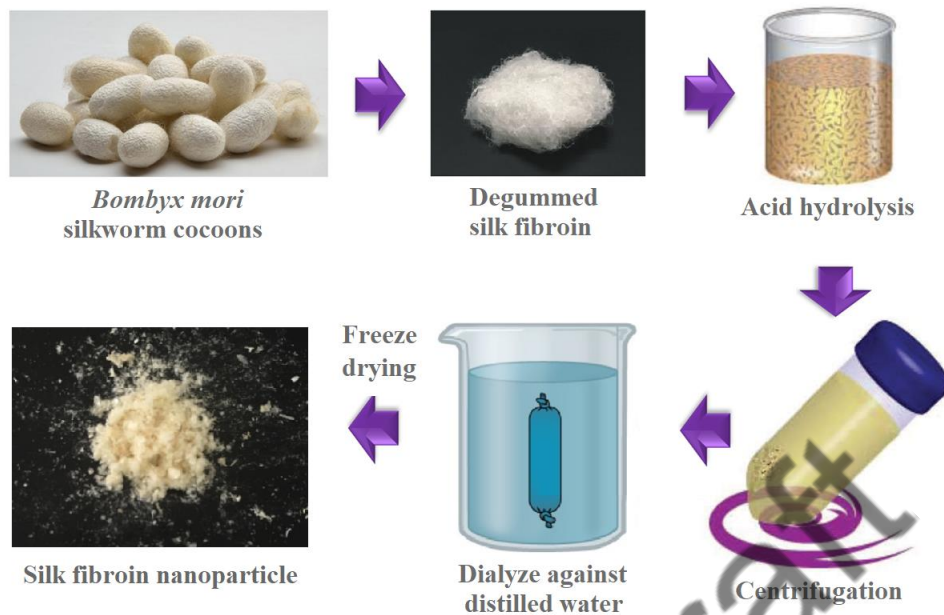
Figure 1. Preparation process of SFNP.

2.3. Preparation of the polymer blends

Prior to processing, milled PLA powder was crystallized, for 20 min at 100 °C [26], and dried for 2 h at 85 °C in a vacuum oven. Moreover, milled PCL powder and SFNP nanoparticle were dried in a vacuum oven at 40 °C and 85 °C for 2 h, respectively. Then, the samples were processed by extrusion using a twin-screw micro compounder (Rondol Microlab, France), with a screw speed of 60 rpm and L/D = 20 [27]. The barrel temperature profile from hopper to die was set at 125, 160, 190, 190, and 180 °C for PLA and PLA/PCL blends, while the temperature profile for the neat PCL samples was 110, 110, 110, 80, and 50 °C [16][28]. Various neat blends of PLA/PCL (100/0, 90/10, 80/20, 70/30, and 0/100), as well as a nanocomposite based on (PLA/PCL; 70/30) containing 1% SFNP, were prepared. Then the obtained filaments were molded into the films with a thickness of ~ 300 μm on a hot press (IQAP-LAP, Spain) at 190 °C.

7

2.4. Characterization techniques

2.4.1. Fourier-transform infrared spectroscopy (FT-IR)

Infrared spectra of the samples were recorded using a Nicolet iS10 spectrometer (USA). Each spectrum was recorded between 400 and 4000 cm^{-1} with a resolution of 4 cm^{-1}. Spectral correction of the FTIR-ATR spectra was done using the software Omnic 9.2.41.

2.4.2. X-ray diffraction (XRD)

X-ray diffraction (XRD) patterns of the samples were measured by X'PERT-MPD (Netherlands) diffractometer, equipped with a CuKa generator (λ_1 = 0.154,056 nm and λ_2 = 0.154,439 nm) at 40 mA and 45 kV, in a 2ϴ range from 1.7 to 40 °.

2.4.3. Thermogravimetric analysis (TGA)

Thermogravimetric analysis (TGA) of the samples was obtained by TA Instruments TGA2050 (USA) thermobalance. The test was carried out in a dry nitrogen atmosphere (30 cm^3/min) between 25 and 800 °C at a heating rate of 10 °C/min.

2.4.4. Differential scanning calorimetry (DSC)

Differential scanning calorimetry (DSC) analysis was performed using the TA Instruments Q-20 (USA) and Mettler Toledo DSC822E (Switzerland) calorimeters. The samples were heated from 20 to 220 °C at 10 °C/min under a nitrogen atmosphere and then kept for 3 min at 220 °C to remove the thermal history. After that, the samples were cooled to 0 °C, and finally, a second heating scan was performed until 220 °C, also at 10 °C/min. To investigate the isothermal crystallization values, the samples were heated from 20 to 220 °C at 10 °C/min and then maintained at 220 °C for 5 min. Subsequently, the samples were rapidly cooled (-50 °C/min) and

8

held at 105 °C for 60 min. The Avrami equation was used to study the crystallization kinetics which is shown below:

$$1 - X_t = \exp(-Z_t t^n) \tag{1}$$

where X_t is the relative degree of crystallinity at the time (t). Moreover, n and Z_t are respectively the Avrami exponent and rate constant, which are calculated from the slope and intercept of the plot of ln (-ln (1-Xt)) vs. ln (t) plot (Equation 2) [29][30]:

$$\ln[-\ln(1 - X_t)] = n \ln(t) + \ln(Z_t) \tag{2}$$

The values of half-time crystallization ($t_{1/2}$) and growth rate (G) are calculated from Equation 3 and 4, respectively.

$$t_{1/2} = \left(\frac{\ln 2}{Z_t}\right)^{1/n} \tag{3}$$

$$G = \left(\frac{1}{t_{1/2}}\right) \tag{4}$$

2.4.5. Scanning electron microscope (SEM)

The morphological observation of the samples was carried out with the scanning electron microscope (SEM) (AIS2100, South Korea) at an accelerating voltage of 15 kV. Before the examination, the fractured surfaces of samples were coated with a thin layer of gold.

2.4.6. Vicker microhardness

The microhardness measurements were measured by Type M Shimadzu microhardness tester (Japan). A Vickers pyramidal indenter was used, applying a load of 25 g for 10 s. Each sample was measured six times.

2.4.7. Water vapor permeability (WVP)

The water vapor permeability (WVP) of the samples was determined according to the UNE 53097 standard (similar to the ISO 2528:2017 standard). Films of the different materials, prepared by casting from their solution in chloroform (1 W/V%), were cut into squares of 5×5 cm and mounted in the permeability cup (VF2200 TQC Sheen BV, Netherlands) together with 2 g of dried silica gel, and then weighed (W_0). After that, the cups were placed in the desiccator at 23±0.5 °C containing a saturated potassium nitrate solution to reach the humidity of ~ 90%. The weights of the cups were measured every hour for 8 h (W_n) and a graph of the entered water (W_n-W_0) versus time was plotted. WVP was calculated using Equation (5):

$$WVP = \frac{240 \times m}{S} \text{ (gr/day.cm}^2)$$
(5)

where m is the slope of the entered water (W_n-W_0) versus time, and S represents the internal area of the cup (10 cm^2). An open cup with the same weight of silica gel was used as a control. Every test was repeated three times and the means values of WVP are reported.

3. Results and Discussion

3.1. Characterization of silk fibroin nanoparticles (SFNP)

3.1.1. FT-IR tests

The FT-IR measurements were used to make sure degummed SF is properly regenerated from the *Bombyx mori* silkworm cocoons. Figure 2a shows the FT-IR spectra of degummed SF and SFNP. Intense absorption bands on the FT-IR spectra of SF were observed for amide I, amide II, and amide III at 1625 cm^{-1}, 1513 cm^{-1}, and 1227 cm^{-1}, respectively. The frequencies of amide regions are in line with the FT-IR spectra of different previous studies [20][31][32]. Another amide I small absorption band is observed at 1699 cm^{-1}, which is the characteristic band of β-sheet structures formed by hydrogen bonding between the C=O and N-H groups [33]. In the FT-IR spectra of SFNP, the amide absorption peaks were observed at 1651 (amide I), 1515 (amide II), and 1232 cm^{-1} (amide III). During acid hydrolysis, the H^{+} ions penetrate into the ordered and unordered domains of SF and short polypeptide chains are formed [24]. The shifting of amide I peak from 1625 cm^{-1} in degummed SF to 1651 cm^{-1} in SFNP reveals a reduction of intermolecular interaction after acid hydrolysis, which could be a consequence of the disordered polymer structure in the nanoparticle [34]. Moreover, the absorption band of the β-sheet crystals, which appears at 1699 cm^{-1} in the SF spectrum, is absent in the SFNP spectrum, thus confirming the transformation of the well-ordered β-sheet crystals in SF into random coil conformations in SFNP [35].

3.1.2. XRD tests

The diffractograms corresponding to SF and SFNP are shown in Figure 2b. The main peaks of SF at 2Θ values of 9.28 and 20.85° correspond to the β-sheet conformation (silk II) and the peak

at $2\Theta = 24.71°$ is attributed to the α-helix/random coil structure (silk I) [36]. The average crystallinity value (x_c) of SF is ~ 55% in the literature data [37]. The two peaks disappeared in the XRD profile of SFNP, thus confirming the change from the ordered domains to amorphous structures that are observed in the FT-IR spectra. As suggested by Um et al., the short order crystals of SF are too small to be detected in the diffractogram of SFNP [38].

3.1.3. Thermal Characterization

The TGA results of SF and SFNP are presented in Figure 2c and Table 1. The thermal degradation of the samples occurred in the range of 250-740 °C having a major peak at ~ 320 °C. The mass loss of 4% below 100 °C could be due to the loss of water. The thermogram of SFNP shifted towards lower temperatures in the onset and end set temperature ranges. Moreover, according to the TGA data, the temperature for 10% weight loss (T_{10}) and maximum-rate degradation (T_{max}) of degummed SF decreased after acid hydrolysis from 294.5 to 266.3 °C and 333.9 to 313.1 °C, respectively. It can be concluded that due to the cleavage of the SF chains upon hydrolysis, SFNP with lower molecular weight exhibited lower thermal stability than the native SF. The strong dependence of the thermal stability on the length of the molecules was reported by Mamun et al. [39].

The DSC results confirmed the difference between the structure of degummed SF and SFNP. The results of the first heating DSC thermograms of SF and SFNP are given in Figure 2d and Table 2. The endothermic shift of the baseline and broad endothermic peak observed at 192.7 and 320.9 °C, are attributed to the glass transition temperature (T_g) and melting temperature (T_m) of SF, respectively. As can be seen, the T_g of SFNP shifted to a lower temperature in comparison with degummed SF. This change indicates that the cleavage of the SF chain increased the

molecular movement. Moreover, T_m downshifted to a lower value, from 320.9 °C (SF) to 307.6 °C (SFNP), which corresponds to the typical temperature of amorphous SF structure [40]. It can be concluded that both the decrease of the interactions between the polymer chains and the decrease of the thermal stability is related to the less ordered arrangement of SFNP macromolecules.
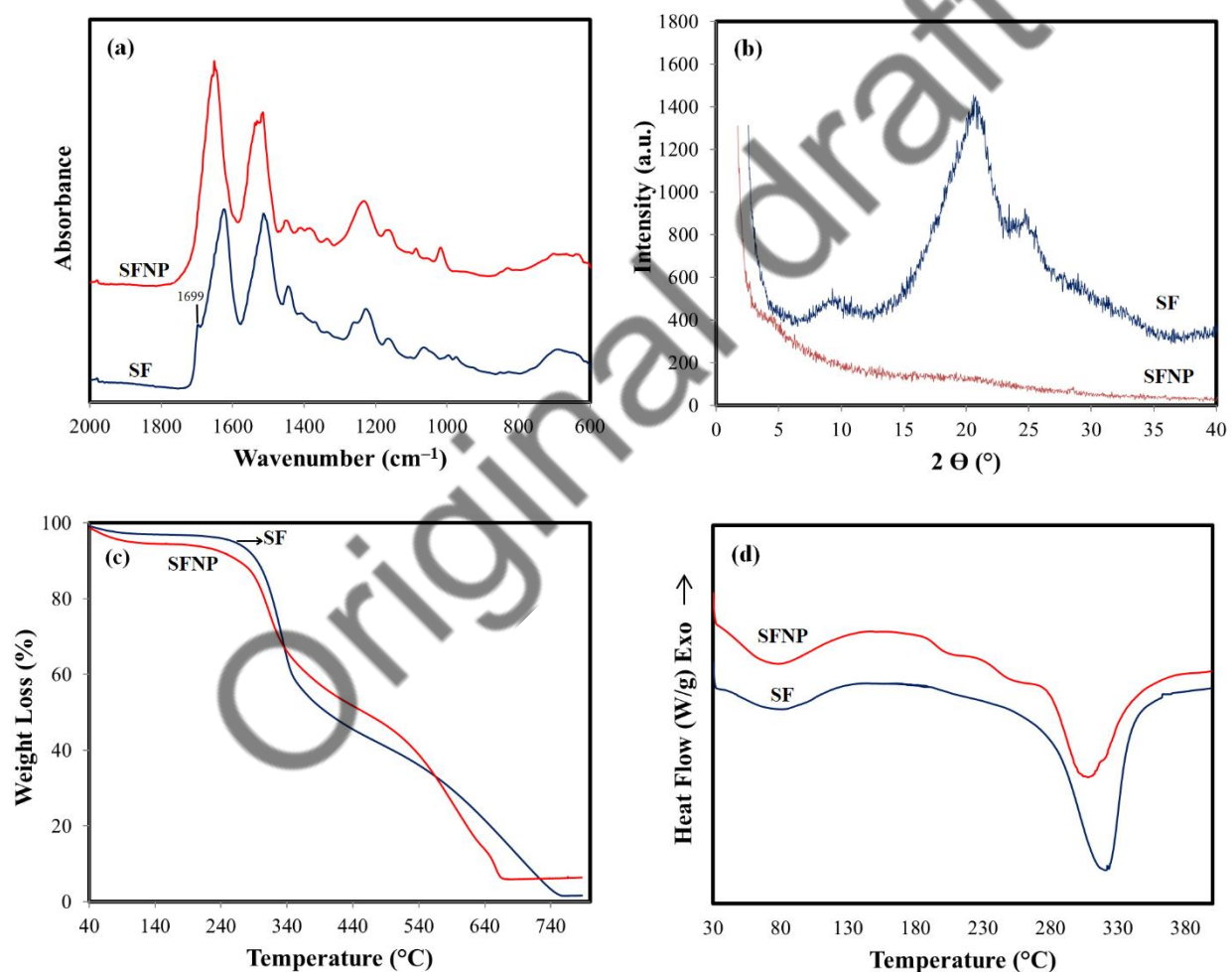

Figure 2. (a) FT-IR spectra, (b) XRD patterns, (c) TGA, and (d) first heating DSC curves of SF and SFNP.

3.2. Characterization of the prepared blends and nanocomposites

3.2.1. Microscopy tests

SEM images representative of the morphology of different samples are presented in Figure 3. A comparative study of the phase morphologies of the samples was performed. Figure 3a shows a smooth microstructure with no irregularities which indicate the brittle nature of the neat PLA. As can be seen in Figure 3b-d, PLA and PCL are incompatible and the PCL droplets appear isolated inside the PLA matrix, as it was previously observed by Wu et al. [14]. With the increase of PCL content in the polymer blends, the bigger PCL domain sizes are observed in the PLA matrix. Additionally, it could be observed that there are many drop-out traces in the fracture surface of the PLA/PCL blends, which shows that the surface roughness was increased in the presence of PCL. This result indicates that a more ductile material was obtained due to the addition of PCL to the PLA matrix, in good agreement with the results reported by Yeh et al. [5]. Figure 3e shows the homogeneous dispersion of SFNP (as shown by the green arrow) in the PLA/PCL (70/30) blend although some agglomerates of SFNP are observed (as shown by the red arrow in the circles). The addition of SFNP leads to a relatively uniform phase morphology of the PLA/PCL blend. A more continuous interface could be observed because of the interaction between the functional groups on the surface of SFNP and the two polymers. Figure 3f shows the mean diameter of PCL domains in different PLA/PCL blends. As can be seen, the PCL domain size decreased upon the addition of SFNP, which demonstrates the compatibilizing effect of nanoparticle. A similar result also was reported by Nematollahi et al. [41], who revealed that the use of nanosilica in the PLA/natural rubber (PLA/NR) blends caused a reduction of the NR droplet sizes. These results indicate that nanoparticle can promote the compatibility between the PLA matrix and dispersed phases. It could be expected the organic nanoparticle to act as a bridge

between the two immiscible components, leading to a better stress transfer and thus an improvement of the mechanical properties of the materials [42].
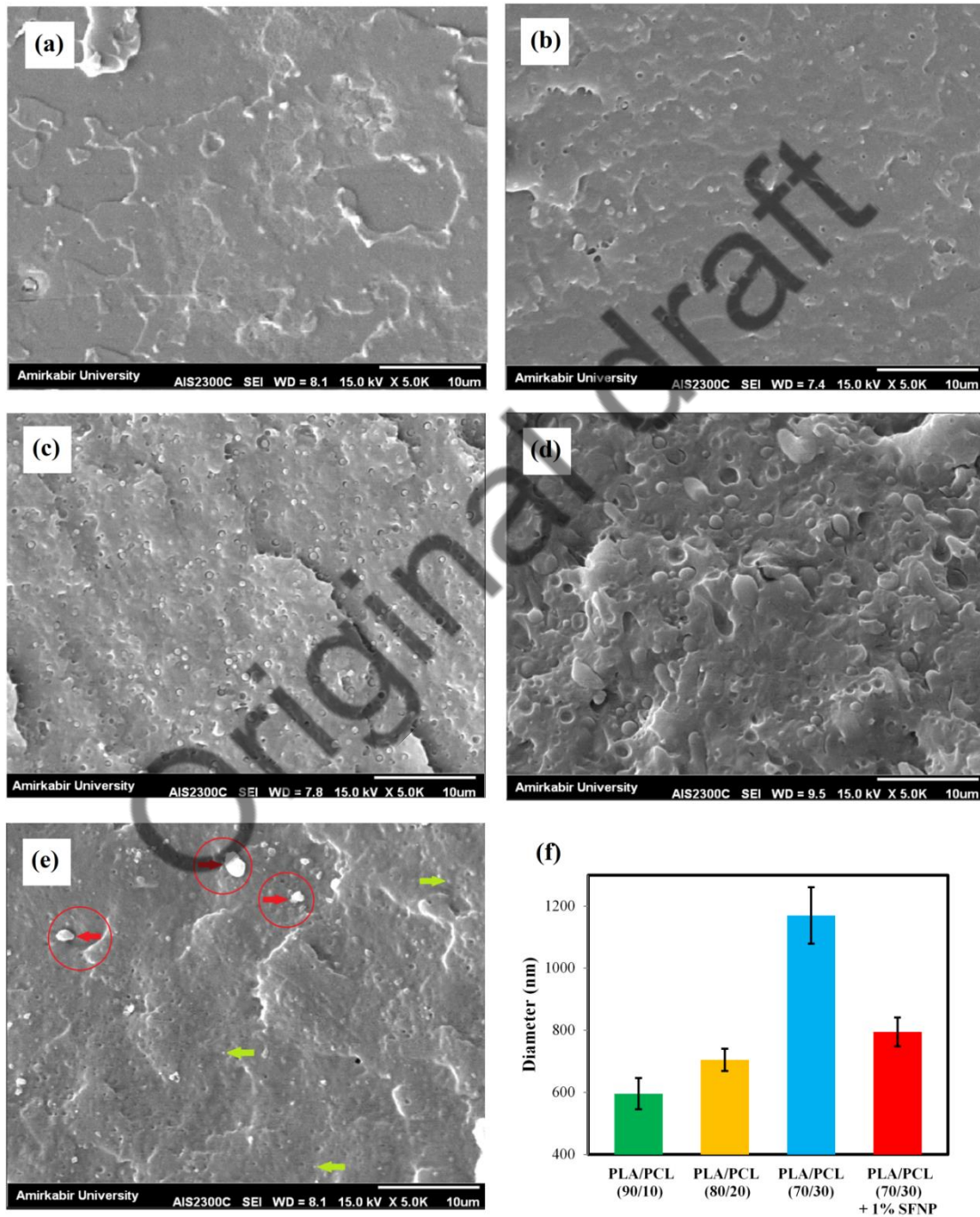
Figure 3. SEM images of: (a) PLA, (b) PLA/PCL (90/10), (c) PLA/PCL (80/20), (d) PLA/PCL (70/30), (e) PLA/PCL/SFNP bio-nanocomposite, and (f) mean diameter of PCL droplets.

3.2.2. FT-IR tests

The FT-IR spectra of the samples are shown in Figure 4. The peaks located at 2995, 2944 and 1755 cm^{-1} in the PLA spectrum, and the peaks at 2946, 2867 and 1727 cm^{-1} in PCL were assigned to the ν_{asC-H}, ν_{sC-H}, and $\nu_{C=O}$ vibrations, respectively [28][43]. The peaks at 1268, 1090 and 868 cm^{-1} that appear in the spectrum of PLA correspond to the ν_{COC}, ν_{sCOC}, and ν_{C-COO} vibrations, respectively [44]. Moreover, the ν_{asCOC} and ν_{OC-O} peaks of PCL can be observed at 1241 and 1190 cm^{-1}, respectively [45]. As expected, the spectra of the blends show that the intensity of the band at 1729 cm^{-1} increases as the PCL content does. According to Hoidy et al. [15], the terminal hydroxyl groups of PLA could form intermolecular hydrogen bonds with the carbonyl groups of PCL, but in these spectra, no additional peaks are observed. Similarly, the amide and hydroxyl groups of SFNP could interact by hydrogen bonds formation with PLA and PCL; however, the FTIR spectrum of the nanocomposite does not show new bands due to those interactions, probably due to the small amount of SFNP present in the material.
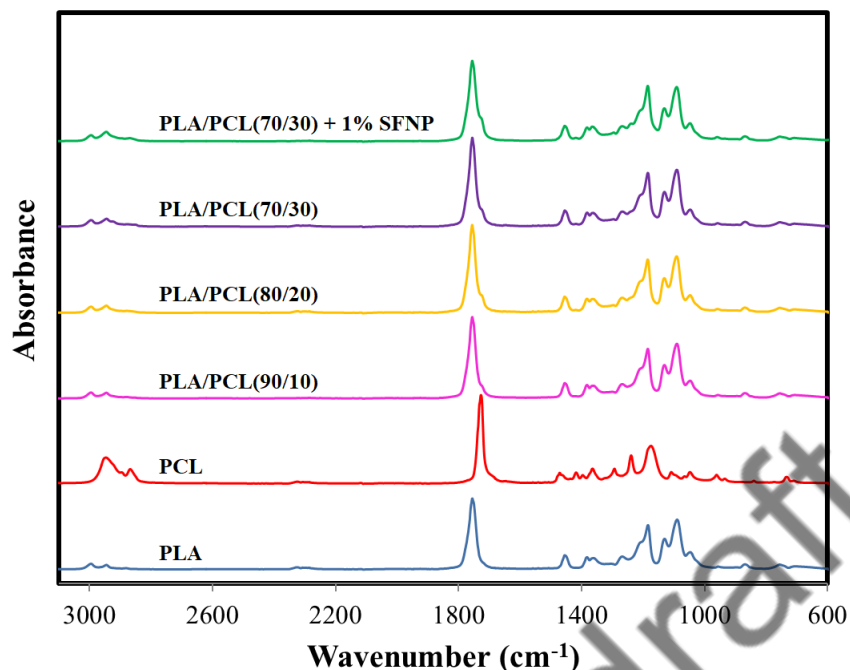
Figure 4. FT-IR spectra of PLA, PCL, PLA/PCL blends, and PLA/PCL/SFNP bio-

nanocomposite.

3.2.3. Thermal analysis

TGA was performed to determine the thermal stability of the investigated samples and the results

are presented in Figure 5a and Table 1. Besides, for better visualization of the degradation

process, the first derivative TGA curves (DTG curves) of the samples are shown in Figure 5b.

Both PLA and PCL were thermally degraded in a single step, with maximum degradation

temperature (T_{max}) located at 374.3 °C and 412 °C, respectively. The initial decomposition

temperature (T_{onset} or T_5) of PLA is 332.1 °C, while that of PCL is 341.6 °C. The thermal

stability of PLA is lower than that of PCL and it decomposed before PCL [46]. The results

indicated that at the onset degradation temperatures, there was no significant difference between

PLA and PLA/PCL blends (p-value > 0.05). However, Table 1 shows that the T_{95} (temperature at 95% mass loss) of PLA was increased with the addition of PCL. It could be concluded that the thermal stability at high temperatures of the PLA/PCL blends increases with the PCL content, in good agreements with previous results of Hoidy et al. [15]. The PLA chains were restricted by PCL with higher thermal decomposition temperature, and consequently, high temperature or more energy is needed to degrade the materials [46]. It could be observed that in the early stages of thermal decomposition (T_5 and T_{10}), the degradation temperature of the PLA/PCL blend decreased upon the incorporation of 1% of SFNP. It might be due to the acid functional groups of SFNP, which increase the degradation rate of the ester bonds in PLA and PCL. A similar result was observed in the case of cellulose nanocrystals (CNC) and PLA. Dhar et al. [47] demonstrated that the sulfate functional groups of the CNC used accelerated the degradation of PLA chains when it was subjected to the extrusion. However, the T_{95} of the PLA/PCL blend was shifted towards a higher value when SFNP was added to the blend. This result can be explained taking into account that the nanoparticle can act as a heat barrier for the PLA and PCL chains improving slightly the thermal stability of the materials in the end set temperature range.
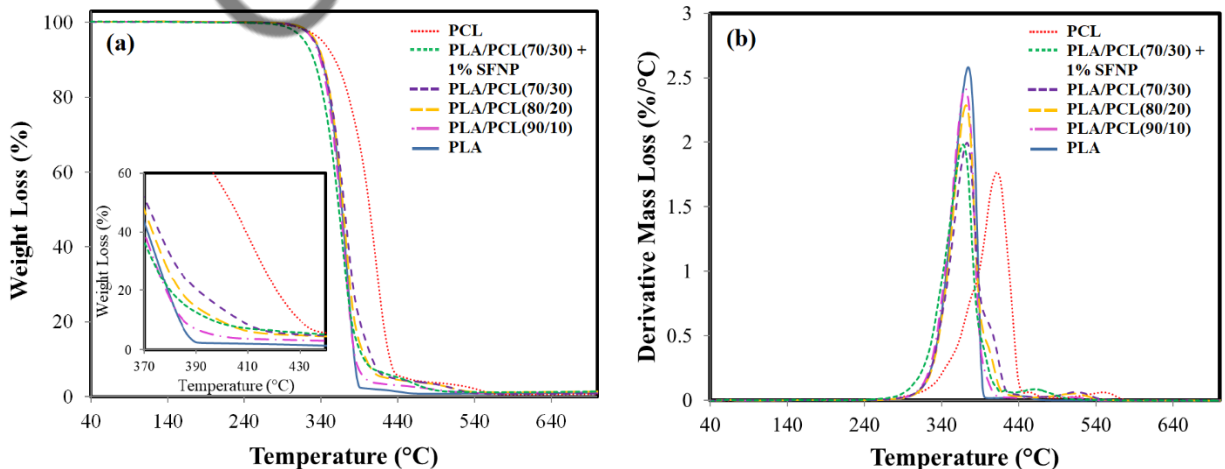
Figure 5. The thermal degradation curves: (a) TGA and (b) DTG of PLA, PCL, PLA/PCL blends, and PLA/PCL/SFNP bio-nanocomposite.

Table 1. Thermal gravimetric analyses data of samples obtained from TGA

Sample	T_5 (°C)	T_{10} (°C)	T_{50} (°C)	T_{max} (°C)	T_{95} (°C)
SF	258.3	294.5	399.6	333.9	728.8
SFNP	107.3	266.3	458.6	313.1	674.2
PLA	332.1	341.4	367.2	374.3	386.6
PCL	341.6	358.3	403.4	412.0	448.1
PLA/PCL (90/10)	330.1	339.3	365.6	370.3	396.4
PLA/PCL (80/20)	333.1	342.4	368.8	371.5	429.1
PLA/PCL (70/30)	331.3	341.1	370.7	372.7	436.0
PLA/PCL (70/30) + 1% SFNP	318.5	330.8	363.2	367.6	443.8

DSC was used to determine the thermal properties and melt/crystallization behavior of the different samples. Figure 6(a) shows the second heating curves of the samples from 0 to 170 °C at 10 °C/min heating rate. The neat PLA showed a glass transition (T_g) at 58.3 °C, a cold crystallization centered at T_{cc} = 112.8 °C, and two melting peaks at 147.8 °C and 153.8 °C, which are consistent with the literature data [27]. The double melting peak of the samples is attributed to the melt recrystallization mechanism that includes the melting of the less perfect crystals at the lower temperature (T_{m1}), their rearrangement into the more ordered structures during the heating, and their melting at the higher temperature (T_{m2}) [28][48][49]. The neat PCL showed a melting peak at 55.8 °C. It is worth to note that due to the overlap of the melting peak

of PCL and the glass transition peak of PLA which is around 60 ºC, it was difficult to determine the T_g of PLA in the blends. As shown in Table 2, the T_{cc} and T_m of PLA in the PLA/PCL blends are essentially unchanged from that of the neat PLA.

Figure 6(b) shows the cooling curve of the samples at 10 °C/min cooling rate from 170 to 0 °C. PCL crystallized completely, while PLA hardly showed any crystallization and no apparent peak was noted. The results imply the different crystallization behavior of these two polymers. The neat PCL showed a sharp crystallization peak (T_c) at 33.3 °C, which shifted to the higher values with increasing the PCL content in the blend. In the study conducted by Matsuba et al. [50], the results showed that the phase separation in the polyolefin blends enhanced the crystal nucleation density and lamella growth [5][15]. Similar results in our research could be explained by this hypothesis. The phase separation area between PLA and PCL acted as an active nuclei substrate in the first crystal nucleation step and facilitated the crystallization process of PCL as PLA content in the blend increased.

The T_g and T_m (Figure 6(a)) of PLA changed insignificantly upon the incorporation of SFNP into the neat PLA. However, the T_{cc} value of PLA decreased from 112.8 to 109.2 °C. This may be attributed to the nucleating effect of SFNP. A similar result was also reported for cellulose-reinforced PLA composites [51]. Regarding the behavior of the PLA/PCL blends, the addition of SFNP to the PLA/PCL (70/30) blend increased the T_{cc} of PLA, along with a decrease of the crystallization enthalpies (ΔH_c) of PCL. This behavior could be due to SFNP acting as a compatibilizer, forming an interfacial bonding between the PLA matrix and PCL dispersed phase. Therefore, the improved intermolecular interaction between polymers resulted in a lower molecular movement, and consequently, polymer chains were more restricted to participate in the crystallization process [42][52].
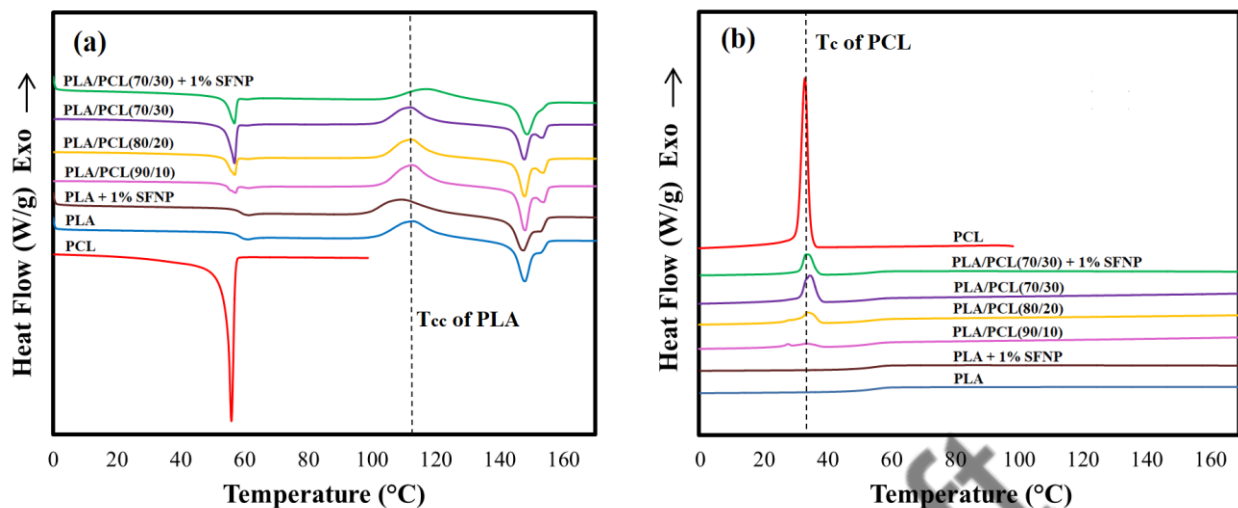
Figure 6. (a) Second heating and (b) cooling DSC scans of PLA, PLA/SFNP, PCL, PLA/PCL blends, and PLA/PCL/SFNP bio-nanocomposite.

Table 2. Thermal parameters of samples from the heating and cooling DSC scans

Sample	T_g (°C)	T_{cc} (°C) (PLA)	T_{m1} (°C)	T_{m2} (°C)	T_c (°C) (PCL)	ΔH_c (J/g) (PCL)	ΔH_{cc} (J/g) (PLA)	ΔH_m (J/g)
SF	195.2	-	320.9	-	-	-	-	372.5
SFNP	192.7	-	307.6	-	-	-	-	214.3
PLA	58.3	112.8	147.8	153.8	-	-	21.6	29.2
PLA + 1% SFNP	58.8	109.2	147.4	153.4	-	-	21.9	28.6
PCL	-	-	55.8	-	33.3	54.1	-	60.4
PLA/PCL (90/10)	-	112.5	147.9	153.7	33.9	4	24.8	26.2
PLA/PCL (80/20)	-	112.2	147.8	153.6	34.1	8.2	22.3	22.8
PLA/PCL (70/30)	-	111.9	147.6	153.4	35	15	21	21.3
PLA/PCL (70/30) + 1% SFNP	-	117	148.6	153.9	34	10.4	16.5	21.2

A kinetic analysis was performed to further study the crystallization behavior and the results are shown in Figure 7 and Table 3. Figure 7(a) illustrates the values of relative crystallinity (X_t) as a function of crystallization time (t) of the samples. The comparison of the curves of PLA and PLA/SFNP, as well as the values of the crystallization half-times ($t_{1/2}$) and the growth rate (G) values indicated a faster crystallization for PLA/SFNP compared to the neat PLA. This confirms the nucleating effect of the nanoparticles, which increases the rate of the crystallization process of PLA [53].

Among the investigated samples (Table 3), the PLA/PCL (70/30) blend exhibited the minimum and maximum values of $t_{1/2}$ (2.92 min) and G (0.34 min^{-1}), respectively. As mentioned earlier, the PCL droplets can act as a nucleating agent for the PLA chains and promote the crystallization process of PLA. The same results were observed for the PLA blended with other polymers [54].

Regarding the effect of SFNP on the behavior of the PLA/PCL blend, Figure 7 shows that, although SFNP acts as a nucleating agent for the neat PLA, the crystallization rate of the nanocomposite is lower than the neat PLA/PCL blend, in good agreement with the dynamic DSC results. However, the value of $t_{1/2}$ is still lower than that of the neat PLA. Figure 7(b) shows the plot of ln (-ln (1-Xt)) as a function of ln (t) for the different samples. The Avrami exponent (n) was calculated from the slope of ln (-ln (1-Xt)) vs. ln (t) plot, and then the n values are provided in Table 3. According to Wurm et al. [55], n = 2 normally indicates the athermal nucleation and growth into two dimensional (2-D) lamellar aggregates, and n = 3 is attributed to the athermal nucleation and growth into three dimensional (3-D) spherulites for slow heating rate. As can be seen in Table 3, the n values are between 3 and 4 for all the samples, which imply the 3-D spherulite crystal growth at a low heating rate that we used in this study (10 °C/min).
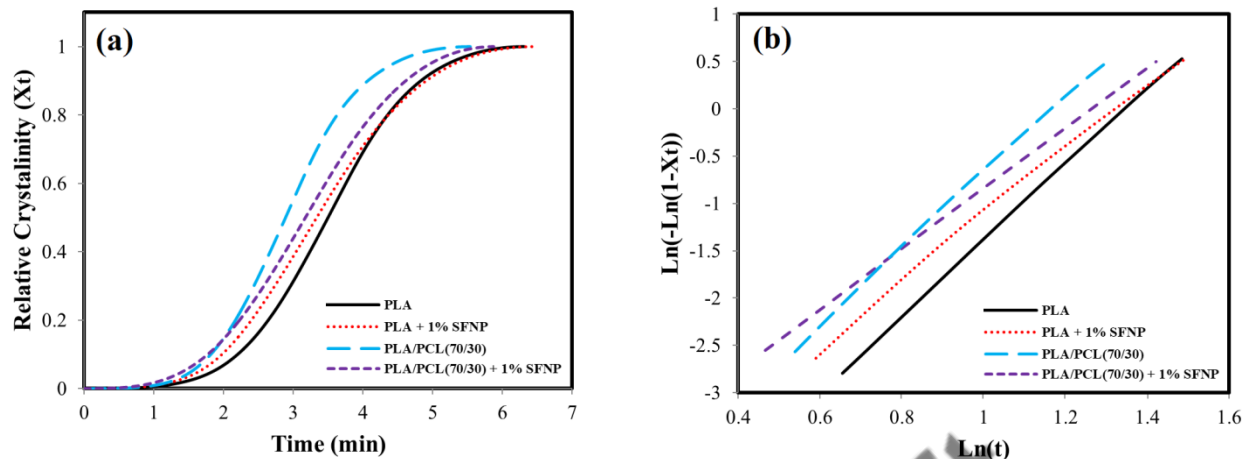
Figure 7. (a) Relative crystallinity vs. time and (b) Avrami plot of ln (-ln (1-Xt)) vs. ln (t) of the

samples.

Table 3. Avrami constants (n and Z_t), crystallization half time (t ½), and growth rate (G) of the

samples

Sample	n	Z_t	$t_{1/2}$ (min)	G (min^{-1})
PLA	4.02	0.0044	3.42	0.29
PLA + 1% SFNP	3.45	0.0104	3.37	0.30
PLA/PCL (70/30)	4.01	0.0093	2.92	0.34
PLA/PCL (70/30) + 1% SFNP	3.19	0.0177	3.18	0.31

3.2.4. Estimation of mechanical properties

To estimate the mechanical properties of the samples, microhardness measurements were carried

out on the different samples and the results are shown in Figure 8. As can be seen, the values of

hardness decreased significantly in direct proportion to the PCL content (p-value < 0.05). This

23

result could be due to the plasticizing effect of PCL for the PLA matrix. Several studies reported that the mechanical properties of PLA can be tuned from rigid to ductile by the addition of PCL [5][26][56][57]. Therefore, the enhancing of chain mobility caused a significant decrease in the microhardness values of the PLA/PCL blends. Furthermore, it can be seen that the incorporation of only 1% of SFNP increased the hardness of the PLA/PCL blend by ~ 9.7%, which is attributed to the reinforcing effect of nanoparticle and the increase of the molecular interaction between the two polymers.
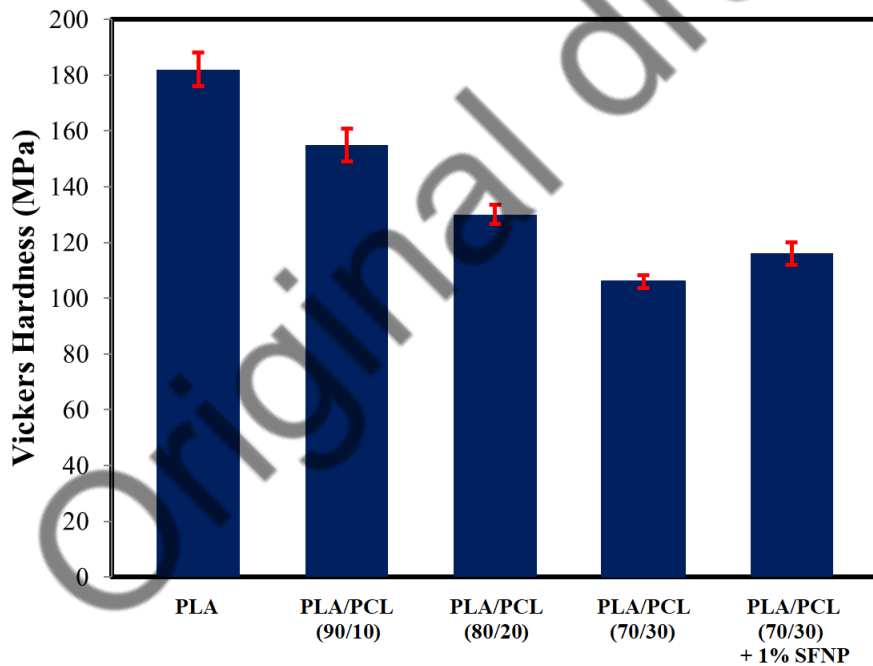

Figure 8. Vickers hardness values of PLA, PLA/PCL blends, and PLA/PCL/SFNP bio-nanocomposite.

3.2.5. Water vapor permeability

Water vapor permeability (WVP) is one of the key properties of polymers in food packaging and other very important applications. The barrier properties can be affected by different parameters such as the crystallinity degree of the materials and the presence of nanoparticles [10]. The WVP determined for the different samples are presented in Figure 9. These results indicate that the permeability of water vapor molecule in the neat PLA/PCL (70/30) blend is significantly higher than that of the neat PLA. This could be attributed to the poor miscibility between the phases since phase separation and voids can create a preferential pathway for transport of water vapor molecules in the immiscible polymer blends [58]. However, by using SFNP in the PLA/PCL blend, the WVP value decreased significantly (decrease of ~ 16%). A similar trend was reported in the literature for PLA reinforced with silk powder [42]. The effect of SFNP can be due, at least in part, to its hydrophobic nature, which difficult the diffusion of moisture from the surroundings. Moreover, it is well known that the increasing of the tortuosity path (due to the presence of nanoparticle) translates into a reduction of the gases and vapors permeability [59]. Therefore, it could be concluded that the network like structures formed between the polymer chains and SFNP restricted the transport rate of water vapor molecules through the sample films.
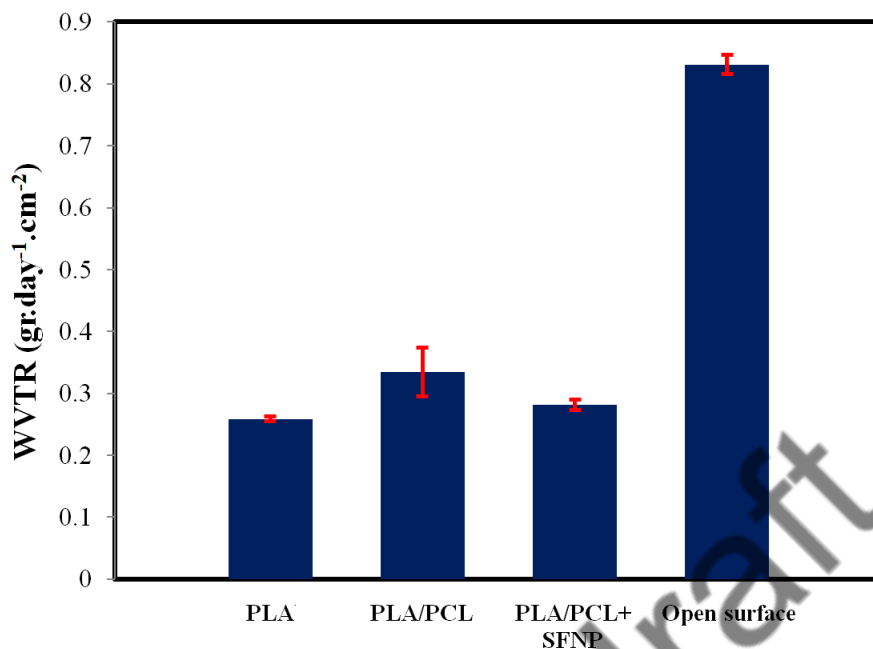
Figure 9. Water vapor transmission rate values of PLA, PLA/PCL (70/30), PLA/PCL/SFNP bio-nanocomposite, and open surface as a control.

4. Conclusions

Blends of PLA/PCL containing different amounts of PCL and a nanocomposite based on (PLA/PCL; 70/30) with 1% SFNP were successfully prepared. The SEM results revealed that the presence of SFNP improved the interfacial adhesion between the polymer phases and decreased the diameter of the PCL droplets in the PLA matrix. The results of TGA showed that the degradation temperature of the polymer blend decreased upon the incorporation of SFNP in the early stages, while, the thermal stability improved slightly in the end set temperature range. The results of the thermal study and crystallization kinetics indicated that both SFNP and PCL acted as active nucleation substrates, promoting the crystallization of the neat PLA. However, the

crystallization rate of the blend containing SFNP was lower than that of the neat blend. This might be due to the increasing intermolecular interactions between the nanoparticle and polymer chains which decelerated the molecular movements and crystallization process. Moreover, based on the microhardness results, an increase in the hardness value could be observed upon the incorporation of SFNP into the PLA/PCL blend. Additionally, the presence of SFNP led to significant improvement in the barrier properties of the blend due to the well dispersion of nanoparticle in the polymer matrix, as suggested by SEM results. Therefore, it could be concluded that the PLA/PCL/SFNP bio-nanocomposites are environmentally-friendly materials for demanding applications such as food packaging.

References

[1]   Wang D, Lu X, Qu J. Role of In situ thermal-reduced graphene oxide on the morphology and properties of biodegradable poly (Lactic acid)/poly (butylene succinate) blends. *Polym Compos*.

[2]   Muller J, González-Mart\'\inez C, Chiralt A. Combination of poly (lactic) acid and starch for biodegradable food packaging. *Materials (Basel)* 2017; 10: 952.

[3]   Bharimalla AK, Deshmukh SP, Vigneshwaran N, et al. Nanocellulose-polymer composites for applications in food packaging: Current status, future prospects and challenges. *Polym Plast Technol Eng* 2017; 56: 805–823.

[4]   Kellersztein I, Amir E, Dotan A. Grafting of wheat straw fibers with poly (ε-caprolactone) via ring-opening polymerization for poly (lactic acid) reinforcement. *Polym Adv Technol* 2016; 27: 657–664.

[5]   Yeh J-T, Wu C-J, Tsou C-H, et al. Study on the crystallization, miscibility, morphology, properties of poly (lactic acid)/poly (ε-caprolactone) blends. *Polym Plast Technol Eng* 2009; 48: 571–578.

[6]   Ojijo V, Sinha Ray S, Sadiku R. Toughening of biodegradable polylactide/poly (butylene succinate-co-adipate) blends via in situ reactive compatibilization. *ACS Appl Mater Interfaces* 2013; 5: 4266–4276.

[7]   Murariu M, Da Silva Ferreira A, Alexandre M, et al. Polylactide (PLA) designed with desired end-use properties: 1. PLA compositions with low molecular weight ester-like plasticizers and related performances. *Polym Adv Technol* 2008; 19: 636–646.

[8]   Cheung H-Y, Lau K-T, Pow Y-F, et al. Biodegradation of a silkworm silk/PLA composite. *Compos Part B Eng* 2010; 41: 223–228.

[9]   Hasook A, Tanoue S, Iemoto Y, et al. Characterization and mechanical properties of poly (lactic acid)/poly (ϵ-caprolactone)/organoclay nanocomposites prepared by melt compounding. *Polym Eng Sci* 2006; 46: 1001–1007.

[10]   Bouakaz BS, Habi A, Grohens Y, et al. Organomontmorillonite/graphene-PLA/PCL

nanofilled blends: New strategy to enhance the functional properties of PLA/PCL blend. *Appl Clay Sci* 2017; 139: 81–91.

[11]   Di Y, Iannace S, Di Maio E, et al. Nanocomposites by melt intercalation based on polycaprolactone and organoclay. *J Polym Sci Part B Polym Phys* 2003; 41: 670–678.

[12]   Pillin I, Montrelay N, Grohens Y. Thermo-mechanical characterization of plasticized PLA: Is the miscibility the only significant factor? *Polymer (Guildf)* 2006; 47: 4676–4682.

[13]   Broz ME, VanderHart DL, Washburn NR. Structure and mechanical properties of poly (D, L-lactic acid)/poly (ε-caprolactone) blends. *Biomaterials* 2003; 24: 4181–4190.

[14]   Wu D, Lin D, Zhang J, et al. Selective localization of nanofillers: effect on morphology and crystallization of PLA/PCL blends. *Macromol Chem Phys* 2011; 212: 613–626.

[15]   Hoidy WH, Ahmad MB, Al-Mulla EAJ, et al. Preparation and characterization of polylactic acid/polycaprolactone clay nanocomposites. *J Appl Sci* 2010; 10: 97–106.

[16]   Decol M, Pachekoski WM, Becker D. Compatibilization and ultraviolet blocking of PLA/PCL blends via interfacial localization of titanium dioxide nanoparticles. *J Appl Polym Sci*; 135.

[17]   Luzi F, Fortunati E, Puglia D, et al. Study of disintegrability in compost and enzymatic degradation of PLA and PLA nanocomposites reinforced with cellulose nanocrystals extracted from Posidonia Oceanica. *Polym Degrad Stab* 2015; 121: 105–115.

[18]   Yang W, Dominici F, Fortunati E, et al. Effect of lignin nanoparticles and masterbatch procedures on the final properties of glycidyl methacrylate-g-poly (lactic acid) films

before and after accelerated UV weathering. *Ind Crops Prod* 2015; 77: 833–844.

[19] Tesfaye M, Patwa R, Kommadath R, et al. Silk nanocrystals stabilized melt extruded poly (lactic acid) nanocomposite films: Effect of recycling on thermal degradation kinetics and optimization studies. *Thermochim Acta* 2016; 643: 41–52.

[20] Dadras Chomachayi M, Solouk A, Akbari S, et al. Electrospun nanofibers comprising of silk fibroin/gelatin for drug delivery applications: Thyme essential oil and doxycycline monohydrate release study. *J Biomed Mater Res - Part A*; 106. Epub ahead of print 2018. DOI: 10.1002/jbm.a.36303.

[21] Chomachayi MD, Solouk A, Mirzadeh H. Mathematical modeling of electrospinning process of silk fibroin/gelatin nanofibrous mat: Comparison of the accuracy of GMDH and RSM models. *J Ind Text* 2019; 1528083719851856.

[22] Kim SH, Nam YS, Lee TS, et al. Silk fibroin nanofiber. Electrospinning, properties, and structure. *Polym J* 2003; 35: 185–190.

[23] Chomachayi MD, Solouk A, Mirzadeh H. Electrospun silk-based nanofibrous scaffolds: fiber diameter and oxygen transfer. *Prog Biomater* 2016; 5: 71–80.

[24] Tao Y, Xu W, Yan Y, et al. Preparation and characterization of silk fibroin nanocrystals. *Polym Int* 2012; 61: 760–767.

[25] Haque MM-U, Puglia D, Fortunati E, et al. Effect of reactive functionalization on properties and degradability of poly (lactic acid)/poly (vinyl acetate) nanocomposites with cellulose nanocrystals. *React Funct Polym* 2017; 110: 1–9.

[26] Beltrán FR, de la Orden MU, Lorenzo V, et al. Water-induced structural changes in poly

(lactic acid) and PLLA-clay nanocomposites. *Polymer (Guildf)* 2016; 107: 211–222.

[27] Beltrán FR, Barrio I, Lorenzo V, et al. Mechanical recycling of polylactide: improvement of the properties of the recycled material.

[28] Beltrán FR, Lorenzo V, de la Orden MU, et al. Effect of different mechanical recycling processes on the hydrolytic degradation of poly (l-lactic acid). *Polym Degrad Stab* 2016; 133: 339–348.

[29] Deroiné M, Le Duigou A, Corre Y-M, et al. Accelerated ageing of polylactide in aqueous environments: comparative study between distilled water and seawater. *Polym Degrad Stab* 2014; 108: 319–329.

[30] Itim B, Philip M. Effect of multiple extrusions and influence of PP contamination on the thermal characteristics of bottle grade recycled PET. *Polym Degrad Stab* 2015; 117: 84–89.

[31] Heseltine PL, Hosken J, Agboh C, et al. Fiber Formation from Silk Fibroin Using Pressurized Gyration. *Macromol Mater Eng* 2018; 1800577.

[32] Di Foggia M, Taddei P, Torreggiani A, et al. SELF-ASSEMBLING PEPTIDES FOR BIOMEDICAL APPLICATIONS: IR AND RAMAN SPECTROSCOPIES FOR THE STUDY OF SECONDARY STRUCTURE. *Proteomics Res J* 2011; 2: 231.

[33] Lu Q, Zhang B, Li M, et al. Degradation mechanism and control of silk fibroin. *Biomacromolecules* 2011; 12: 1080–1086.

[34] Noishiki Y, Nishiyama Y, Wada M, et al. Mechanical properties of silk fibroin--microcrystalline cellulose composite films. *J Appl Polym Sci* 2002; 86: 3425–3429.

[35] Chomachayi MD, Solouk A, Mirzadeh H. Improvement of the Electrospinnability of Silk Fibroin Solution by Atmospheric Pressure Plasma Treatment. *Fibers Polym* 2019; 20: 1594–1600.

[36] Wang R, Pu D, Dong Y, et al. Silk fibroin powder prepared by nontoxic low-sodium salt system. *Mater Lett* 2017; 206: 5–8.

[37] Trabbic KA, Yager P. Comparative structural characterization of naturally-and synthetically-spun fibers of Bombyx mori fibroin. *Macromolecules* 1998; 31: 462–471.

[38] Um IC, Kweon H, Park YH, et al. Structural characteristics and properties of the regenerated silk fibroin prepared from formic acid. *Int J Biol Macromol* 2001; 29: 91–97.

[39] Mamun A, Rahman SMM, Roland S, et al. Impact of Molecular Weight on the Thermal Stability and the Miscibility of Poly (ε-caprolactone)/Polystyrene Binary Blends. *J Polym Environ* 2018; 26: 3511–3519.

[40] Magoshi J, Nakamura S. Studies on physical properties and structure of silk. Glass transition and crystallization of silk fibroin. *J Appl Polym Sci* 1975; 19: 1013–1015.

[41] Nematollahi M, Jalali-Arani A, Modarress H. Effect of nanoparticle localization on the rheology, morphology and toughness of nanocomposites based on poly (lactic acid)/natural rubber/nanosilica. *Polym Int* 2019; 68: 779–787.

[42] Patwa R, Kumar A, Katiyar V. Effect of silk nano-disc dispersion on mechanical, thermal, and barrier properties of poly (lactic acid) based bionanocomposites. *J Appl Polym Sci* 2018; 135: 46671.

[43] Ghasemi-Mobarakeh L, Prabhakaran MP, Morshed M, et al. Bio-functionalized PCL

nanofibrous scaffolds for nerve tissue engineering. *Mater Sci Eng C* 2010; 30: 1129–1136.

[44]   Edith D, Six J-L, others. Surface characteristics of PLA and PLGA films. *Appl Surf Sci* 2006; 253: 2758–2764.

[45]   Elzein T, Nasser-Eddine M, Delaite C, et al. FTIR study of polycaprolactone chain organization at interfaces. *J Colloid Interface Sci* 2004; 273: 381–387.

[46]   Chen C-C, Chueh J-Y, Tseng H, et al. Preparation and characterization of biodegradable PLA polymeric blends. *Biomaterials* 2003; 24: 1167–1173.

[47]   Dhar P, Tarafder D, Kumar A, et al. Thermally recyclable polylactic acid/cellulose nanocrystal films through reactive extrusion process. *Polymer (Guildf)* 2016; 87: 268–282.

[48]   Yu L, Liu H, Dean K, et al. Cold crystallization and postmelting crystallization of PLA plasticized by compressed carbon dioxide. *J Polym Sci Part B Polym Phys* 2008; 46: 2630–2636.

[49]   Di Lorenzo ML. Calorimetric analysis of the multiple melting behavior of poly (L-lactic acid). *J Appl Polym Sci* 2006; 100: 3145–3151.

[50]   Matsuba G, Shimizu K, Wang H, et al. The effect of phase separation on crystal nucleation density and lamella growth in near-critical polyolefin blends. *Polymer (Guildf)* 2004; 45: 5137–5144.

[51]   Suryanegara L, Nakagaito AN, Yano H. The effect of crystallization of PLA on the thermal and mechanical properties of microfibrillated cellulose-reinforced PLA composites. *Compos Sci Technol* 2009; 69: 1187–1192.

33

[52]   Li H, Huneault MA. Effect of nucleation and plasticization on the crystallization of poly (lactic acid). *Polymer (Guildf)* 2007; 48: 6855–6866.

[53]   Papageorgiou GZ, Achilias DS, Bikiaris DN, et al. Crystallization kinetics and nucleation activity of filler in polypropylene/surface-treated SiO2 nanocomposites. *Thermochim Acta* 2005; 427: 117–128.

[54]   Shin BY, others. Viscoelastic properties of PLA/PCL blends compatibilized with different methods. *Korea-Australia Rheol J* 2017; 29: 295–302.

[55]   Wurm A, Zhuravlev E, Eckstein K, et al. Crystallization and homogeneous nucleation kinetics of poly (ε-caprolactone)(PCL) with different molar masses. *Macromolecules* 2012; 45: 3816–3828.

[56]   Tsuji H, Ikada Y. Blends of aliphatic polyesters. I. Physical properties and morphologies of solution-cast blends from poly (DL-lactide) and poly (ε-caprolactone). *J Appl Polym Sci* 1996; 60: 2367–2375.

[57]   Jelcic Z, Holjevac-Grguric T, Rek V. Mechanical properties and fractal morphology of high-impact polystyrene/poly (styrene-b-butadiene-b-styrene) blends. *Polym Degrad Stab* 2005; 90: 295–302.

[58]   Moustafa H, Galliard H, Vidal L, et al. Facile modification of organoclay and its effect on the compatibility and properties of novel biodegradable PBE/PBAT nanocomposites. *Eur Polym J* 2017; 87: 188–199.

[59]   Chen J-H, Chen C-C, Yang M-C. Characterization of nanocomposites of poly (butylene adipate-co-terephthalate) blending with organoclay. *J Polym Res* 2011; 18: 2151–2159.